

OccluTrack: Rethinking Awareness of Occlusion for Enhancing Multiple Pedestrian Tracking

Jianjun Gao, Yi Wang, Kim-Hui Yap, Kratika Garg, and Boon Siew Han

Abstract—Multiple pedestrian tracking faces the challenge of tracking pedestrians in the presence of occlusion. Existing methods suffer from inaccurate motion estimation, appearance feature extraction, and association due to occlusion, leading to inadequate Identification F1-Score (IDF1), excessive ID switches (IDSw), and insufficient association accuracy and recall (AssA and AssR). We found that the main reason is abnormal detections caused by partial occlusion. In this paper, we suggest that the key insight is explicit motion estimation, reliable appearance features, and fair association in occlusion scenes. Specifically, we propose an adaptive occlusion-aware multiple pedestrian tracker, OccluTrack. We first introduce an abnormal motion suppression mechanism into the Kalman Filter to adaptively detect and suppress outlier motions caused by partial occlusion. Second, we propose a pose-guided re-ID module to extract discriminative part features for partially occluded pedestrians. Last, we design a new occlusion-aware association method towards fair IoU and appearance embedding distance measurement for occluded pedestrians. Extensive evaluation results demonstrate that our OccluTrack outperforms state-of-the-art methods on *MOT-Challenge* datasets. Particularly, the improvements on IDF1, IDSw, AssA, and AssR demonstrate the effectiveness of our OccluTrack on tracking and association performance.

Index Terms—Multiple pedestrian tracking, tracking by detection, Kalman filter, re-identification, data association

I. INTRODUCTION

MULTIPLE pedestrian tracking is a challenging task aiming to form trajectories for detected pedestrians over time. This process involves detecting pedestrians and associating identical pedestrians from sequential frames. It is important in various real-world applications such as surveillance [1], [2], robotics [3], [4], and autonomous driving [5], [6].

Existing state-of-the-art multiple pedestrian tracking methods [7]–[10] associate detected pedestrians by combining cues like motions and appearance features to address the occlusion problem. Kalman Filter, one of the motion estimators, is commonly used to provide motion cues by formulating multiple pedestrian tracker as a linear estimation problem, which recursively predicts and updates trajectories from noisy observations (detections) over frames. Re-ID modules extract appearance features from multiple frames to identify the same pedestrian. However, these methods, even with re-ID, are insufficient to resolve occlusion problems because of inaccurate motion estimates, unreliable appearance features, and unfair association.

Recently, occlusion has drawn much attention in multiple pedestrian tracking, and various approaches were proposed to address this issue, e.g., tracking by attention [11]–[13], graph

neural networks [14], self and cross-attention mechanism [15]–[18], and hierarchical feature extraction [19]. They address the occlusion problem by formulating motion patterns via advanced deep learning models in adjacent or multiple frames [11], [15], [16], [18] or understanding the context information in the scene [14], [17], [19]. However, these methods require significant computation resources compared with the Kalman Filter, and they ignore the effects caused by partial occlusion.

Through visualization of experimental results, we found partial occlusion is the missing key to resolving the occlusion problem. Partial occlusion creates abnormal bounding boxes covering some body parts only. These abnormal bounding boxes change suddenly in center points and aspect ratios, which causes “inaccurate motion estimates”, appearance features, and associations. As shown in Fig. 1(a), abnormal detections caused by partial occlusion mislead the motion estimator in predicting wrong trajectories. Especially the errors will be accumulated and amplified without accurate observations during full occlusion. As for re-ID modules, the inputs are from the cropped images according to the detections. Nevertheless, the cropped images will cover two persons (part of the obscured and part of the visible person) during partial occlusion, introducing “unreliable and noisy appearance features”. Moreover, the predictions from the motion estimator during occlusion are not as accurate as those in normal situations because of the error accumulation caused by partial occlusion. Hence, the association method should not treat occluded persons as strictly as visible persons, i.e., “unfair association”.

To alleviate the three problems caused by partial occlusions, we propose the OccluTrack, an adaptive occlusion-aware multiple pedestrian tracker with three strategies, as shown in Fig. 1(b). First, we propose an abnormal motion suppression mechanism for stabilizing parameter updates in the Kalman Filter. In particular, the abnormal motion suppression mechanism leverages the history of tracked persons’ observations to detect and suppress abnormal motions. The motion can be more accurately predicted by abnormal motion suppression when partial occlusion occurs. Second, we introduce a pose-guided re-ID strategy for robust part feature extraction. The pose-guided re-ID strategy utilizes a pose estimator to guide the feature extractor to obtain more discriminative features. Lastly, we adopt an occlusion-aware distance measurement for occluded person association. The occlusion-aware distance measurement strategy involves a combination of IoU distance and appearance embedding distance under adaptive thresholds based on the level of occlusion, which is fair for occluded pedestrians.

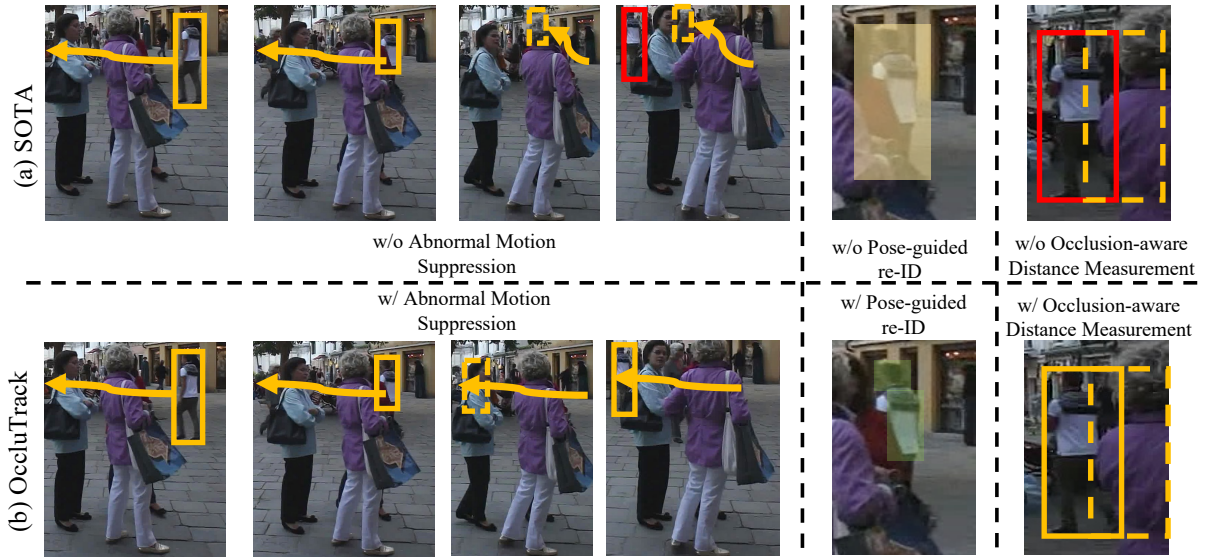


Fig. 1. The motivation of our proposed OccluTrack. (a) Left: SOTA trackers struggle with abnormal motions caused by partial occlusion, leading to inaccurate motion estimation. Middle: They also lack pose guidance during partial occlusion, resulting in unreliable appearance features. Right: Treating occluded and non-occluded pedestrians equally in distance measurement hinders optimal association. (b) In contrast, OccluTrack incorporates abnormal motion suppression (left), pose-guided re-ID (middle), and occlusion-aware distance measurement (right) to address these limitations.

We apply our method to three baseline trackers (JDE [20], FairMOT [8], and BoT-SORT [10]), showing that the IDF1 and IDSw on the MOT17 validation set are improved consistently from 1.5% to 2.4% and 15% to 30%, respectively. We also evaluated our OccluTrack on the *MOTChallenge* datasets, and the results show that our method outperforms other approaches by a significant margin. Compared with the state-of-the-art BoT-SORT [10], the average improvement on IDF1 and IDSw reaches 1.0% and 12.5% on MOT17 and MOT20 test sets. Meanwhile, the improvements in AssA and AssR show a better association ability compared with other methods. Especially on the MOT20 dataset, AssA and AssR increase by 2.7% and 1.7% respectively. Our contributions can be summarized as follows:

- 1) We propose the Kalman Filter with an abnormal suppression mechanism to explicitly alleviate abnormal motions caused by partial occlusion.
- 2) We introduce a pose-guided re-ID to extract more discriminative and reliable appearance features for partially occluded pedestrians.
- 3) We propose an occlusion-aware distance measurement method to make the association fair for occluded pedestrians.
- 4) Our proposed OccluTrack outperforms the state-of-the-art methods on MOTChallenge datasets, showing better tracking and association performance.

II. RELATED WORK

A. Multiple Pedestrian Tracking

At the early stage, works on multiple pedestrian tracking mainly focus on solving occlusion problems by motion cues. Intuitively, IoUTrack [21] associates the tracklets and detection solely based on the IoU. Only the IoU distance for detections

from two adjacent frames indicates the geometric similarity. SORT [7] was the first work introducing Kalman Filter as the motion estimator into tracking-by-detection methods. Unlike IoUTrackers, SORT can predict the current positions upon the motion cues generated from Kalman Filter and enhance the tracking performance during occlusion. ByteTrack [9] and OC-SORT [22] promoted the SORT by associating almost every detected object and smoothing the Kalman Filter by observations. Apart from SORT-based methods, CenterTrack [23] built on CenterNet [24] adopts a regressor as the motion estimator, which regresses object motions from two adjacent frames. Following works [25]–[28] make CenterTrack more robust by introducing more proper motion formulation methods like incorporating past detections, cost volume, and Quasi-Dense similarities. STTD [29] detects pedestrians with topologies and learns the dynamics of moving pedestrians within the same topology group.

Motion cues are not enough for occlusion avoidance because of a lack of accurate observations. The appearance feature [30] is another cue to address the occlusion problem. DeepSort [31] first introduced re-ID to solve the occlusion using appearance features. Following works [8], [10], [20], [32]–[36] adopt embedded or stand-by more robust re-ID modules to enhance the ability to resolve the occlusion problem by modeling re-ID more accurately. However, appearance features vary in different scenarios, especially during partial occlusion.

Besides, some tracking-by-attention [11]–[13], [37], [38] methods modify DETR [39], [40] to an end-to-end tracker by introducing tracking queries and detection queries for tracked objects and new-born objects. These tracking-by-attention methods lack motion cues, which are sensitive to occlusions. Methods like P3AFormer [41] re-introduce motion cues by methods like optical flows. Some other methods solve the occlusion problem from aspects of learning long-term

temporal features and understanding scenes. DeepTracklet and MotionTrack [15]–[18] make use of self- or cross-attention to learn long-term features. TransMOT [14] and Quo Vadis [19] try to understand scenes from the perspective of graphs and Bird-Eye-View. However, these methods usually take dramatic computation resources and ignore the effects caused by partial occlusion.

B. Kalman Filter

Kalman Filter is commonly used in multiple pedestrian tracking with a data association algorithm such as the nearest neighbor and Hungarian algorithms. Data association algorithms associate the observations with the predicted states, and the Kalman Filter updates the state estimates based on the associations. It is a recursive algorithm that estimates the state of a system based on noisy observations. It consists of two main steps: the prediction step and the update step. The two predictions are given by Eq.(1). At each time step t , the Kalman Filter first predicts the state of the system $\hat{x}_{t|t-1}$ using the previous state estimate $\hat{x}_{t-1|t-1}$. And matrix A is the state-transition matrix that relates the state at time $t-1$ to the state at time t . Additionally, the Kalman Filter also predicts the covariance of the state estimate $P_{t|t-1}$ using the previous covariance estimate $P_{t-1|t-1}$ and a process noise Q that describes how the uncertainty in the state evolves.

$$\text{Predict : } \begin{cases} \hat{x}_{t|t-1} = A\hat{x}_{t-1|t-1} \\ P_{t|t-1} = AP_{t-1|t-1}A^T + Q \end{cases} \quad (1)$$

After predicting the state and covariance estimates, the Kalman Filter updates them based on the current observation (or measurement) z_t , as formulated by Eq.(2). The observation model relates the observation to the state $z_t = Hx_t + v_t$, where H is the observation matrix that maps the state to the observation space, and v_t is the observation noise with the covariance matrix of R . The Kalman gain K_t is first calculated in the update step, which determines the weight given to the observation. The updated state estimate $x_{t|t}$ and covariance estimate $P_{t|t}$ are then computed. I is the identity matrix.

$$\text{Update : } \begin{cases} K_t = P_{t|t-1}H^T(H P_{t|t-1}H^T + R)^{-1} \\ \hat{x}_{t|t} = \hat{x}_{t|t-1} + K_t(z_t - H\hat{x}_{t|t-1}) \\ P_{t|t} = (I - K_tH)P_{t|t-1} \end{cases} \quad (2)$$

III. METHODOLOGY

A. Overview

Fig. 2 illustrates the overview of our proposed OccluTrack built upon the baseline tracker, BoT-SORT [10]. To enhance the tracking performance during occlusion, we introduce three components: abnormal motion suppression-based Kalman Filter, pose-guided re-ID, and occlusion-aware distance measurement. For the update component in Fig. 2(c), we propose an abnormal motion suppression mechanism in the Kalman Filter. It first detects abnormal motions by the difference between the current speed and a residual speed from a speed filter. Based on the difference, it determines a dynamic suppression parameter to suppress the outlier motions in the update step

of the Kalman Filter. For the re-ID component in Fig.2(a), our OccluTrack incorporates a pose-guided re-ID module for robust appearance feature extraction. Our pose-guided re-ID extracts local and global features with pose guidance and combines them with an adaptive fusion operation. For the association component in Fig. 2(b), we introduce an occlusion-aware distance measurement to facilitate fair and accurate association of occluded persons by leveraging an adaptive threshold based on occlusion situations. We will elaborate on them in the following sections.

We present the tracking algorithm for our proposed OccluTrack, as shown in Algorithm 1. The algorithm is based on BoT-SORT [10] and adopts the proposed pose-guided re-ID (*PG_ReID*), occlusion-aware distance measurement (*ODM*), and Kalman Filter with abnormal motion suppression (*KF_AMS*) modules indicated by the green comments. The algorithm begins with initializing the tracklets $T = [T_b, T_E, BF_B]$ with $[\emptyset, \emptyset, \emptyset]$ for bounding boxes, feature embeddings, and buffer of the tracked bounding boxes. Next, each frame from a video clip is processed sequentially. For every frame v in video clip V , we perform a pedestrian detection method (*Det*) to obtain the bounding boxes B . These bounding boxes are divided into high-score detections B_h and low-score detections B_l based on their confidence scores. For B_h , we extract the corresponding regions from the frame and feed them into the *PG_ReID* module, as shown in Fig.2(a), to compute the feature embeddings E . In the prediction of Kalman Filter, we predict the bounding boxes T_B for the tracklets in the current frame and perform motion compensation as BoT-SORT [10]. In data association, illustrated in Fig.2(b), we calculate the distance matrix \hat{d}_h via the *ODM* for high-score detections with embeddings. The Hungarian algorithm is then employed to find the indices for matched tracklets and detections, as well as unmatched tracklets and detections. For low-score detections and unmatched tracklets from the previous step, we compute the distance matrix \hat{d}_l using the IoU distance metric to determine the matched and unmatched indices by the Hungarian algorithm. As shown in Fig.2(c), we update *KF_AMS* parameters and bounding box buffer BF_B for the tracklets with matched high-score detections and embeddings, as well as update *KF_AMS* parameters and bounding box buffer BF_B for the tracklets with matched low-score detections according to matched indices. Remained tracklets that are untracked for a duration exceeding a threshold are removed, while new tracklets are initialized for remaining detections B^{remain} if their confidence score exceeds a threshold θ_{new_track} .

B. Abnormal Motion Suppression

a) *Partial Occlusion in Kalman Filter*: In the update step of the Kalman Filter, we find that the observation z_t is incorrect during partial occlusion due to abnormal detections, i.e., suddenly becoming small of objects' bounding boxes caused by partial occlusion. We assume that z_t is corrupted by an error e_t , i.e., $z'_t = z_t + e_t$, where z'_t is the corrupted observation. Hence, the updated state estimate in Eq.(2) becomes:

$$\tilde{x}_{t|t} = \hat{x}_{t|t-1} + K_t(z_t + e_t - H\hat{x}_{t|t-1}) = \hat{x}_{t|t} + K_t e_t, \quad (3)$$

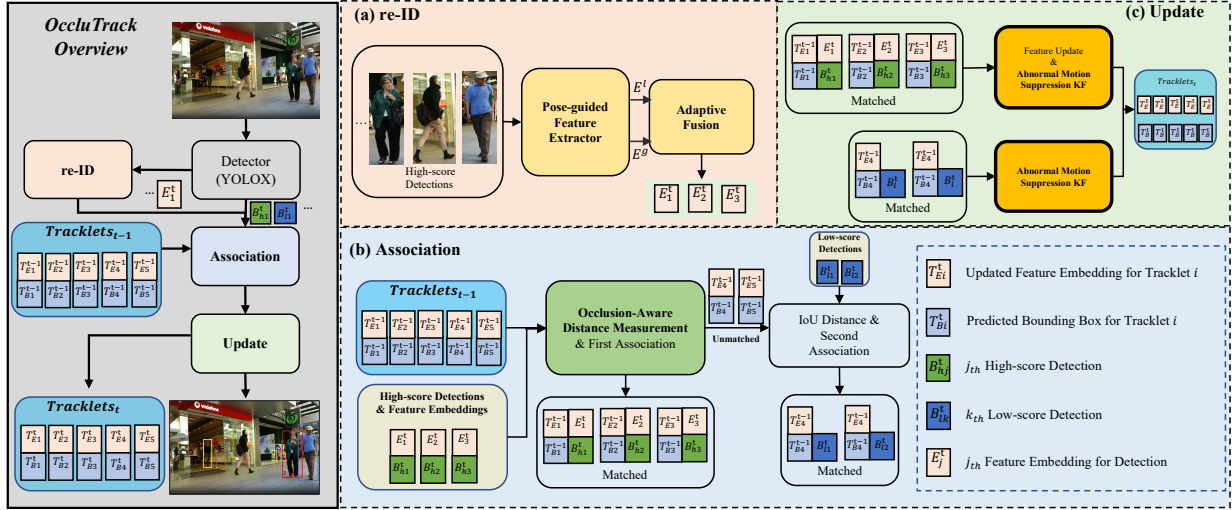


Fig. 2. Overview of our proposed tracker. First, we utilize YOLOX [42] as the object detector to obtain bounding boxes and separate them into high-score and low-score detections. For high-score detections, the re-ID module is used to extract appearance features. Second, the association module is to associate the tracklets of previous frames with the high-score detections (with feature embeddings) and low-score detections of current frames sequentially. Finally, the Kalman Filter (KF) is updated based on the matching results obtained from the association step. Additionally, the appearance features are updated based on the matching results. We highlight three main contributions (components) for MOT: abnormal motion suppression of KF in (c), pose-guided re-ID in (a), and occlusion-aware distance measurement in (b).

where $\tilde{x}_{t|t}$ is the corrupted state estimate disturbed by the $K_t e_t$, and $x = [x, y, w, h, \dot{x}, \dot{y}, \dot{w}, \dot{h}]^T$ representing the position of the bounding box $[x, y, w, h]^T$ and its moving speed $[\dot{x}, \dot{y}, \dot{w}, \dot{h}]^T$. During partial occlusion, the error $e'_t = K_t e_t = [e'_{xt}, e'_{yt}, e'_{wt}, e'_{ht}, e'_{\dot{x}t}, e'_{\dot{y}t}, e'_{\dot{w}t}, e'_{\dot{h}t}]^T$ will dominate the update process. Subsequently, this error will accumulate during full occlusion without observations. In this period, the Kalman filter's state update only relies on the predictions from Kalman Filter. Here, we denote the duration for the full occlusion as τ . As Eq.(1) indicates, the state is predicted by $\hat{x}_{t|t-1} = A\hat{x}_{t-1|t-1}$, where A is the $n \times n$ transition matrix for the state from $t-1$ to t . Formally, A can be elaborated for the linear motion as

$$A = \begin{bmatrix} 1 & 0 & 0 & 0 & 1 & 0 & 0 & 0 \\ 0 & 1 & 0 & 0 & 0 & 1 & 0 & 0 \\ 0 & 0 & 1 & 0 & 0 & 0 & 1 & 0 \\ 0 & 0 & 0 & 1 & 0 & 0 & 0 & 1 \\ 0 & 0 & 0 & 0 & 1 & 0 & 0 & 0 \\ 0 & 0 & 0 & 0 & 0 & 1 & 0 & 0 \\ 0 & 0 & 0 & 0 & 0 & 0 & 1 & 0 \\ 0 & 0 & 0 & 0 & 0 & 0 & 0 & 1 \end{bmatrix}_{8 \times 8}. \quad (4)$$

When the person re-appears after occlusion of τ from t_0 , with only the prediction of the Kalman Filter, the estimate can be predicted like :

$$\begin{aligned} \tilde{x}_{t_0+\tau} &= A^\tau \tilde{x}_{t_0} = A^\tau (\hat{x}_{t_0} + K_{t_0} e_{t_0}) \\ &= \hat{x}_{t_0+\tau} + A^\tau K_{t_0} e_{t_0} = \hat{x}_{t_0+\tau} + A^\tau e'_{t_0}. \end{aligned} \quad (5)$$

According to the transition matrix A and error e'_t , we can obtain A^τ and e'_{t_0} as

$$A^\tau = \begin{bmatrix} 1 & 0 & 0 & 0 & \tau & 0 & 0 & 0 \\ 0 & 1 & 0 & 0 & 0 & \tau & 0 & 0 \\ 0 & 0 & 1 & 0 & 0 & 0 & \tau & 0 \\ 0 & 0 & 0 & 1 & 0 & 0 & 0 & \tau \\ 0 & 0 & 0 & 0 & 1 & 0 & 0 & 0 \\ 0 & 0 & 0 & 0 & 0 & 1 & 0 & 0 \\ 0 & 0 & 0 & 0 & 0 & 0 & 1 & 0 \\ 0 & 0 & 0 & 0 & 0 & 0 & 0 & 1 \end{bmatrix}_{8 \times 8}, \quad (6)$$

$$e'_{t_0} = [e'_{x_0}, e'_{y_0}, e'_{w_0}, e'_{h_0}, e'_{\dot{x}_0}, e'_{\dot{y}_0}, e'_{\dot{w}_0}, e'_{\dot{h}_0}]^T. \quad (7)$$

Hence, the accumulated error $A^\tau e'_{t_0}$ can be calculated by

$$A^\tau e'_{t_0} = \begin{bmatrix} e'_{x_0} + \tau e'_{\dot{x}_0} \\ e'_{y_0} + \tau e'_{\dot{y}_0} \\ e'_{w_0} + \tau e'_{\dot{w}_0} \\ e'_{h_0} + \tau e'_{\dot{h}_0} \\ e'_{\dot{x}_0} \\ e'_{\dot{y}_0} \\ e'_{\dot{w}_0} \\ e'_{\dot{h}_0} \end{bmatrix} \quad (8)$$

From Eq.(8), we can observe that the bounding box $[x, y, w, h]^T$ is shifted by a fixed error $[e'_{x_0}, e'_{y_0}, e'_{w_0}, e'_{h_0}]^T$ and an accumulated error $[\tau e'_{\dot{x}_0}, \tau e'_{\dot{y}_0}, \tau e'_{\dot{w}_0}, \tau e'_{\dot{h}_0}]^T$ with a factor of τ .

b) *Kalman Filter Re-modeling*: It is important to ensure that the observation error should be properly modeled and accounted for in Kalman Filter. To suppress abnormal motions during partial occlusion, we propose an abnormal motion suppression mechanism into Kalman Filter to detect and remove abnormal motions caused by partial occlusion. In particular, at Frame t , we first adopt a memory buffer to collect recent $N+1$ bounding boxes of a tracked pedestrian from $(t-N)$

Algorithm 1: Pseudo-code of OccluTrack

Input: A video sequence V ; object detector Det ; Detection score threshold θ_{det} ; Pose-guided reID PG_ReID ; Kalman Filter with Abnormal Motion Suppression KF_AMS ; Occlusion-aware distance measurement ODM ; Threshold for initializing new tracklets θ_{new_track}

Output: Tracklets $T = [T_B, T_E, BF_B]$ of the video
 // T_B : bounding boxes in tracklets, T_E : feature embeddings in tracklets, BF_B : buffer for tracked bounding boxes

Initialization: $T \leftarrow [\emptyset, \emptyset, \emptyset]$;

```

for v in V do
    B ← Det(v);
    Bh ← ∅; // Initialize high-score bounding boxes
    Bl ← ∅; // Initialize low-score bounding boxes
    for b in B do
        if b.score > θdet then
            Bh ← Bh ∪ {b};
        else
            Bl ← Bl ∪ {b};
        end
    end
    // Pose-guided re-ID
    for b in Bh do
        X = crop(v, b);
        E ← PG_ReID(X, b);
    end
    // Kalman filter prediction
    for tB in TB do
        tB = KF_AMS.predict(tB);
        tB = MotionCompensation(tB, W); // W: warp matrix from t-1 to t
    end
    // Occlusion-aware distance measurement for data association
    dh = ODM(TB, TE, Bh, E); // Associate T and Bh with ODM
    matchedh, unmatchedh = Hungarian(dh);
    dl = IoU_Distance(TB[unmatchedh[0, :]], Bl);
    // Associate remained T and Bl
    matchedl, unmatchedl = Hungarian(dl);
    // Kalman filter update with abnormal motion suppression
    for [i, j] in matchedh do
        KF_AMS.update(TB[i], Bh[j], BF_B[i]);
        TE[i] = (1 - β) * TE[i] + β * E[j];
    end
    for [i, j] in matchedl do
        KF_AMS.update(TB[i], Bl[j], BF_B[j]);
    end
    T ← T \ Tremain; // Remove remained tracklets
    Tremain if untracked for a period
    // Initialize new tracks by remained detections Bremain via θnew_track
    for b in Bremain do
        if b.score > θnew_track then
            T ← T ∪ {b};
        end
    end
end
Return T
    
```

to t , denoted as $\{B^t\}_{t=t-N}^t$ where $B^t = [x, y, w, h]^T$ is a bounding box. Here, we apply a speed filter to calculate the averaged speed of the previous $(N - 1)$ bounding boxes:

$$\bar{v} = \frac{1}{N-1} \sum_{n=t-N+1}^{t-1} (B^n - B^{n-1}), \quad (9)$$

The current speed can be calculated by $v^t = B^t - B^{t-1}$, where $v = [v_x, v_y, v_w, v_h]^T$. We define the speed of the center point and aspect ratio as $v_c = [v_x, v_y]^T$ and $v_a = [v_w, v_h]^T$, respectively. Then, we calculate the difference between the normalized current speed and the normalized average speed in the center point and aspect ratio, i.e., $d_c = \|v_c^t\| - \|\bar{v}_c\|$ and $d_a = \|v_a^t\| - \|\bar{v}_a\|$. Finally, we obtain the speed difference for frame t by $d^t = [d_c^T; d_a^T]^T = [d_x, d_y, d_w, d_h]^T$.

With d^t , we can set a threshold θ_v to detect the abnormal center point moving and scale changing of a tracked person. Afterward, we suppress the Kalman gain in the update step, Eq.(2), to handle the detected abnormal motions caused by the observation error (e_t) during partial occlusion. Formally, we calculate the suppression coefficients $\{\alpha_x, \alpha_y, \alpha_w, \alpha_h\}$ for each element of d^t by:

$$\alpha_i = \begin{cases} 1, & \text{if } d_i^t \leq \theta_v \\ \alpha_0, & \text{otherwise} \end{cases}, \quad (10)$$

where $\alpha_0 < 1$ is a hyper-parameter to perform suppression. The average suppression coefficient $\alpha = (\alpha_x + \alpha_y + \alpha_w + \alpha_h)/4$ is used to scale the Kalman gain of the update step, so the updated state estimate in Eq. (2) is reformulated by:

$$\tilde{x}_{t|t} = \hat{x}_{t|t-1} + \alpha K_t (z_t - H \hat{x}_{t|t-1}) + \alpha K_t e_t. \quad (11)$$

With the suppression coefficient, the model suppresses the state estimate by $\alpha < 1$ when abnormal motions occur ($e_t > 0$), more trusting the predicted state $\hat{x}_{t|t-1}$, and keeps the state estimate by $\alpha = 1$ in normal motions ($e_t = 0$).

While addressing the challenge of error accumulation within the Kalman Filter, OC-SORT [22] concentrates on updating the Kalman Filter solely when pedestrian tracking can resume post occlusion. This approach places emphasis on incorporating velocity costs derived from previous observations into the association cost for updates. However, a notable drawback of this method is its tendency to overlook the impact of abnormal observations. By solely relying on observations, OC-SORT fails to account for the potential inaccuracies introduced by these abnormal observations, especially during instances of partial occlusion. This limitation becomes evident through the resulting significant disparities in velocities, leading to inaccurate association costs and, consequently, inaccurate associations.

In contrast, our proposed approach, OccluTrack, takes a distinct direction by focusing on mitigating the error accumulation issue during partial occlusion itself rather than merely after its occurrence. The central premise of OccluTrack is to rectify the adverse effects introduced by abnormal occlusions. This innovative approach aims to yield superior motion estimation accuracy during occlusion periods.

C. Pose-guided re-ID

a) *Partial Occlusion in re-ID*: In multiple pedestrian tracking, re-ID modules in prior works normally treated the bounding boxes equally using global features regardless of obscured pedestrians or not. They overlooked the significance of local features that contain more identity information, particularly during partial occlusion. Some methods [43] employed Mask-RCNN [44] to extract local features, but they

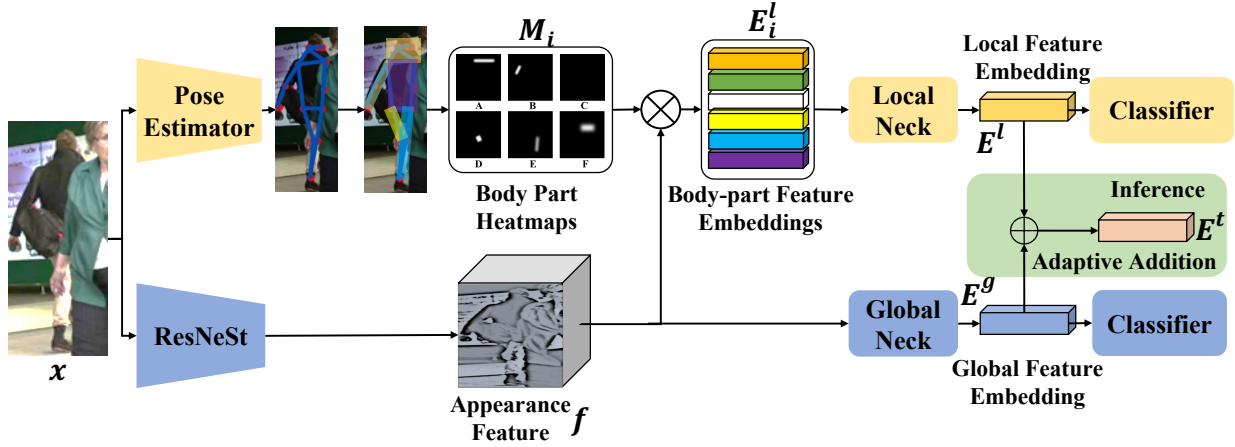


Fig. 3. Architecture of our proposed pose-guided re-ID module. It first extracts appearance features from the cropped image and estimates the pose of the occluded person. After that, body-part features are generated by applying body-part heatmaps to appearance features. By utilizing our proposed local and global necks, local and global feature embeddings are obtained for training. With the adaptive fusion, local and global embeddings are combined for inference.

are coupled with detectors and challenging to optimize. In contrast, our approach introduces a pose-guided re-ID module to adaptively fuse local and global features according to the confidence of body parts, generating more informative person appearance representations.

b) Pose-guided Feature Extractor: As depicted in Fig.3, we combine a real-time pose estimator with the re-ID model to obtain and fuse local body-part and global feature embeddings. Given a high-score bounding box B_h^l , we crop the persons from the input image as the input for the re-ID model. From the figure, the lower-stream ResNeSt [45] extracts the appearance feature $f \in \mathbb{R}^{H \times W \times C}$, where H and W denote the height and width of the feature map, and C represents the channel size. Simultaneously, the upper-stream fast pose estimator [46] produces a heatmap $h \in \mathbb{R}^{H \times W \times 17}$ after Gaussian blur, indicating 17 keypoint positions and confidence scores. To reduce computation complexity, we group the heatmap $h \in \mathbb{R}^{H \times W \times 17}$ into the body-part heatmap $h' \in \mathbb{R}^{H \times W \times 6}$ by summation, as illustrated in Fig.4. Consequently, we use the heatmap to create six masks $hm_i \in \mathbb{R}^{H \times W \times 1}$, where $i \in [0, 5]$. Each mask is repeated in channels, producing a mask of $M_i \in \mathbb{R}^{H \times W \times C}$. Six body-part feature maps f_i^l are obtained by $f_i^l = f \otimes M_i$, where \otimes is the Hadamard product. The body-part feature embedding $E_i^l \in \mathbb{R}^C$ is generated by $E_i^l = \sum_{h=1}^H \sum_{w=1}^W f_i^l(h, w, c)$.

We design local and global necks to extract the local and global feature embeddings. In the local neck, we concatenate the six body-part feature embeddings into $E_c^l = [(E_0^l)^T; (E_1^l)^T; \dots; (E_5^l)^T]^T$ and employ a fully-connected layer to project the channels from $6 \times C$ to C , resulting in a local feature embedding E^l . Conversely, the global neck applies the global average pooling for the appearance feature f , producing a global feature embedding $E^g \in \mathbb{R}^C$. During training, we employ two classifiers with batch normalization for the global and local feature embeddings. The Cross-Entropy loss and Triplet loss serve as the loss functions for each classifier, and we sum the four losses to form the overall

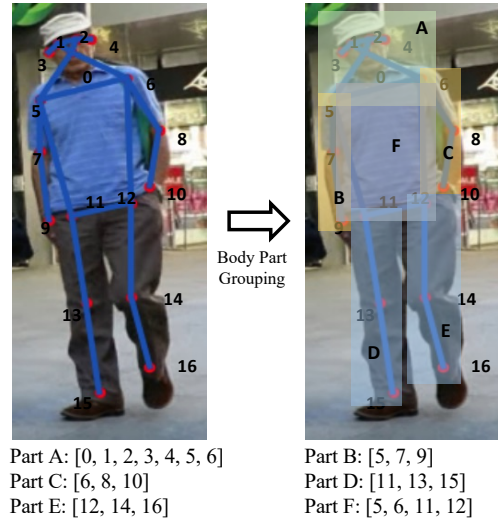


Fig. 4. Combination of body keypoints to form different body parts. The keypoints are grouped into six body parts according to given rules.

loss during training:

$$\mathcal{L} = \mathcal{L}_l^{ce} + \mathcal{L}_l^{triplet} + \mathcal{L}_g^{ce} + \mathcal{L}_g^{triplet}. \quad (12)$$

c) Adaptive Fusion: During inference, feature embeddings associate tracklets appearance-wise by calculating the cosine similarity between the current feature embeddings and those from the previous tracklets. Thus, we should combine the local and global feature embeddings into one embedding before association. We propose an adaptive fusion method to combine local and global feature embeddings according to body-part confidence scores. The insight is to use the confidence scores of body parts to decide the weight of the local features, $n_p \in [0, 6]$. The n_p is obtained by counting the number of body parts whose confidence scores are higher than the threshold θ_p . The adaptive fusion combines two embeddings with the weight (n_p):

$$E^t = \frac{n_p}{6} * E^l + \frac{6 - n_p}{6} * E^g. \quad (13)$$

D. Occlusion-aware Distance Measurement

a) *Partial Occlusion in Data Association:* In state-of-the-art trackers, like BoT-SORT [10], the IoU and appearance feature distances are performed conditionally. Specifically, the IoU and appearance embedding distances are first calculated between the high-score detections with feature embeddings and the tracklets. Conditioning on the IoU distance larger than a threshold, the final distance is chosen from the smaller one between the IoU distance and appearance feature distance. However, the IoU distance is usually inaccurate because of error accumulation during partial occlusion, as mentioned in Section III-B.

b) *Distance Measurement:* To address the issue, we treat the observed tracklets and occluded tracklets in different manners. We adopt the occlusion-aware distance thresholds for two different types of tracklets. For observed tracklets, we keep the same settings as in BoT-SORT. For occluded tracklets, we set a higher IoU distance threshold (θ_i^{iou}) and make it easier to keep track of occluded persons when the bounding boxes re-appear. Formally,

$$\theta_i^{iou} = \begin{cases} \theta_0 & \text{if } i \in I_t \\ \theta_0 + o & \text{if } i \in I_{ut} \end{cases}, \quad (14)$$

where $o > 0$ is the offset for the distance threshold, i is the index for all tracklets, I_t includes indices for tracked tracklets, I_{ut} includes indices for untracked tracklets, and θ_i^{iou} represents the IoU distance threshold for Tracklet i . Then, we calculate the IoU distance $d_{i,j}^{iou}$ between Tracklet i and Detection j and the appearance embedding distance $\hat{d}_{i,j}^{cos}$ by:

$$\hat{d}_{i,j}^{cos} = \begin{cases} d_{i,j}^{cos}, & \text{if } d_{i,j}^{cos} < \theta^{emb} \cap d_{i,j}^{iou} < \theta_i^{iou} \\ 1, & \text{otherwise} \end{cases}, \quad (15)$$

where θ^{emb} is the proximity threshold of appearance embedding distance. Finally, the occlusion-aware distance measurement is obtained by:

$$\hat{d}_{i,j} = \min(d_{i,j}^{iou}, \hat{d}_{i,j}^{cos}). \quad (16)$$

IV. EXPERIMENTS

A. Dataset

We evaluate our proposed method on two multiple pedestrian tracking datasets, MOT17 and MOT20. The MOT17 dataset consists of 14 training and 12 testing video sequences, with over 7 hours of video footage. The videos were captured in various real-world scenarios, such as outdoor scenes, crowded public places, and indoor environments. The dataset contains more than 22,000 annotated pedestrian trajectories, with varying levels of occlusion, illumination changes, and other challenging factors. The MOT20 dataset contains 14 training and 11 testing video sequences, with over 9 hours of video footage. The videos were captured in similar scenarios as MOT17 but with improved annotation quality. The dataset contains over 60,000 annotated object trajectories, with challenging scenarios such as object interactions, fast motion, and occlusions.

TABLE I

THE RESULTS OF COMPONENTS ABLATION STUDY ON THREE DIFFERENT EXISTING TRACKERS OVER MOT17 VALIDATION SET. MS KF MEANS OUR ABNORMAL MOTION SUPPRESSION KALMAN FILTER. PG RE-ID STANDS FOR POSE-GUIDED RE-ID. OD MEA. IS OUR PROPOSED OCCLUSION-AWARE DISTANCE MEASUREMENT.

Tracker	MS KF	PG re-ID	OD Mea.	IDF1 (%) \uparrow	IDS w \downarrow
JDE				63.6	473
	\checkmark			66.2	356
	\checkmark	\checkmark		66.6	347
	\checkmark	\checkmark	\checkmark	66.9	327
FairMOT				72.8	299
	\checkmark			74.9	268
	\checkmark	\checkmark		74.7	223
	\checkmark	\checkmark	\checkmark	74.8	227
BoT-SORT				81.5	147
	\checkmark			82.3	134
	\checkmark	\checkmark		82.7	129
	\checkmark	\checkmark	\checkmark	83.0	125

B. Evaluation Metrics

For both MOT17 and MOT20 datasets, we adopt CLEAR metrics introduced in [47]. The metrics include multiple object tracking accuracy (MOTA), IDF1 score, higher-order tracking accuracy (HOTA), false positive (FP), false negative (FN), ID switch (IDS w), association accuracy (AssA), and association recall (AssR). More importantly, MOTA evaluates the detection performance, IDF1 tests the performance of tracking, and HOTA is a more balanced evaluation metric of detection and tracking. FP and FN indicate the total number of false positives and false negatives. IDS w is the number of ID switches in the whole video. AssA and AssR evaluate the ability of association performance in terms of accuracy and recall.

C. Experimental Settings

We adopt YOLOX as the object detector following the settings in our baseline, where YOLOX is trained on multiple datasets [48]–[51]. As for the parameters in our proposed method, we set the $\alpha_0 = 0.2$ in Eq.(10). And we set the buffer size of the bounding boxes the same as the buffer size for feature embeddings. And we adopt the FastPose in Alphapose [46] as the pose estimator to extract the heatmaps. We adopt ResNest [45] as the appearance feature extractor in pose-guided re-ID. And we follow the training strategies in our baseline for our pose-guided re-ID module. We train the re-ID model for 60 epochs based on the first half of the MOT17 and MOT20 training sets. And during training, the pose estimator is frozen and only provides the heatmaps. In the occlusion-aware distance measurement, we set the offset $o = 0.2$ in Eq.(14). For other parameters, we keep the same settings in our baseline, where the $\theta^{cos} = 0.25$ and $\theta^{iou} = 0.5$. Before submitting results to MOTChallenge, we also perform interpolation on the trajectories following our baseline [10].

D. Ablation Study

a) *Components Analysis:* We assess the impacts of our proposed components on tracking performance of three existing trackers: JDE, FairMOT, and BoT-SORT. We conduct

our experiments on MOT 17 validation set following the strategies in ByteTrack [9]. By gradually incorporating the three components, we evaluate the improvements achieved by each component cumulatively. The results of our ablation study are summarized in Table I, where we bold the best results and highlight the second best in blue.

To begin, we replace the original Kalman Filter in all three trackers with our abnormal motion suppression Kalman Filter. The results demonstrate notable performance gains compared to the original trackers. Applying abnormal motion suppression Kalman Filter to JDE, the IDF1 improves by 2.6% compared to the original JDE, and the IDSw decreases dramatically from 473 to 356. FairMOT also benefits from our proposed Kalman Filter, with IDF1 improvements of 2.1% and a drop in IDSw of 31, achieving the best IDF1 of 74.9%. BoT-SORT also exhibits improved performance, with IDF1 and IDSw showing enhancements of 1% and 8.8%, respectively. These results indicate that our abnormal motion suppression Kalman Filter contributes to better tracking performance across the evaluated trackers.

Next, we apply our pose-guided re-ID module on all three trackers. The results presented in Table I demonstrate that the pose-guided re-ID module primarily impacts the number of IDSw. For JDE, compared to the previous step, the IDSw shows a further improvement of 2.5%. In FairMOT, the performance on avoiding IDSw improves dramatically by 16.8%. Similarly, in BoT-SORT, the number of IDSw drops from 134 to 129, indicating a 3.7% improvement. These findings highlight the efficacy of our pose-guided re-ID module in reducing IDSw and enhancing tracking performance.

Finally, we incorporate our occlusion-aware distance measurement into the three trackers. Notably, this component contributes to the IDF1, as observed in all three trackers. The IDF1 shows improvement across the board, with particularly promising results in BoT-SORT, where the IDF1 reached 83.0%. As for IDSw, improvements are made except for FairMOT. The main reason is that FairMOT adopts a center-based object detector, which is sensitive to IoU distance. Overall, the results demonstrate the effectiveness of our occlusion-aware distance measurement in handling occluded pedestrians and improving tracking performance.

b) Speed Filter: We investigate the impact of alternative speed filters on our tracker’s performance, which are the Gaussian filter, Laplacian filter, and Mean Average filter. Each filter is applied to smooth the buffered centering moving and scale-changing speeds. The Gaussian filter convolves the buffered speeds with a Gaussian kernel, effectively smoothing the centering moving speed and scale-changing speed. The Laplacian filter employs a weighted average of neighboring speeds to smooth the buffered speeds based on their distances. Finally, the Mean Average filter computes the average of all the buffered speeds, as described in Section III-B. We summarize the comparisons among these filters based on the MOT17 validation set in Table II. The results in Table II indicate that our proposed Mean average filter yields the best performance in terms of IDF1 and IDSw. This filter achieves the highest accuracy in estimating pedestrian moving speeds, leading to improved tracking performance.

TABLE II
ABLATION STUDY ON THREE SPEED FILTERS OVER MOT17 VALIDATION SET.

Filter	IDF1(%)↑	IDSw↓
Laplacian	82.6	136
Gaussian	82.8	126
Mean Average	83.0	125

TABLE III
ABLATION STUDY ON FEATURE EMBEDDING FUSION METHODS OVER MOT17 VALIDATION SET.

Fusion	IDF1(%)↑	IDSw↓
Addition	82.8	126
Concatenate	82.8	126
Adaptive Fusion	83.0	125

c) Feature Embedding Fusion: We analyzed the impact of different feature embedding fusion methods on the performance of OccluTrack. The evaluated fusion techniques included addition, concatenation, and our proposed adaptive fusion. The results on the MOT17 validation set, presented in Table III, indicate that the adaptive fusion method outperformed the addition and concatenation methods, demonstrating its effectiveness in improving tracking performance.

d) Abnormal Motion Suppression Parameter: In this section, we ablate the abnormal motion suppression parameter α_0 on the MOT17 validation set. We vary α_0 from 0 to 1 with step 0.1 and evaluate its impact on the tracking performance. $\alpha_0 = 0$ means the Kalman Filter does not update when abnormal motions are detected, while $\alpha_0 = 1$ means the Kalman Filter does not suppress abnormal motions and operates as the normal Kalman Filter. The results are illustrated in Fig.5. When increasing α_0 from 0 to 0.2, we observe that the IDF1 reached the highest at $\alpha_0 = 0.2$ and MOTA increased from the lowest 76.4% at $\alpha_0 = 0$ to the highest 77.3% at $\alpha_0 = 0.2$. Further increasing α_0 leads to a gradual decline in IDF1 and reaches its lowest 81.5% at $\alpha_0 = 1.0$, while MOTA remains relatively stable and ranges between 77.2% and 77.3%. Based on these findings, we set $\alpha_0 = 0.2$ for evaluating the MOT17 and MOT20 test sets.

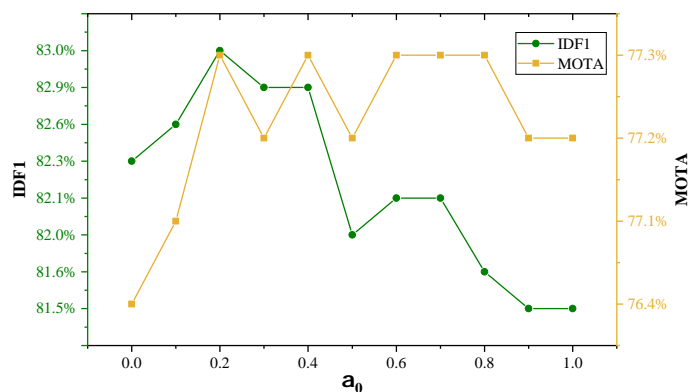


Fig. 5. Illustration of the IDF1 and MOTA during adjusting abnormal motion suppression parameter α_0 .

TABLE IV

EVALUATION RESULTS AND COMPARISONS WITH THE STATE-OF-THE-ART-TRACKERS ON MOT17 TEST SET UNDER PRIVATE DETECTION PROTOCOLS.

Tracker	IDF1 \uparrow	HOTA \uparrow	MOTA \uparrow	FP \downarrow	FN \downarrow	IDSw \downarrow	AssA \uparrow	AssR \uparrow
STTD [29]	51.9	-	54.2	11435	244443	2735	-	-
QuasiDense [27]	66.3	53.9	68.7	26589	146643	3378	52.7	57.2
FairMOT [8]	72.3	59.3	73.7	27507	117477	3303	58.0	63.6
TransCenter [36]	62.2	54.5	73.2	23112	123738	4614	49.7	54.2
TransTrack [13]	63.5	54.1	75.2	50157	86442	3603	47.9	57.1
CSTrack [52]	72.6	59.3	74.9	23847	114303	3567	57.9	63.2
RelationTrack [53]	74.7	61.0	73.8	27999	118623	1374	61.5	67.3
TransMOT [14]	75.1	61.7	76.7	36231	93150	2346	59.9	66.5
FDTrack [33]	75.6	61.3	76.8	34467	92718	3705	-	-
MOTFR [32]	76.3	61.8	74.4	32397	109245	2625	62.6	67.8
OCSORT [22]	77.5	63.2	78.0	15129	107055	1950	63.2	67.5
StrongSORT++ [34]	79.5	64.4	79.6	27876	86205	1194	64.4	71.0
ByteTrack [9]	77.3	63.1	80.3	25491	83721	2196	62.0	68.2
Quo Vadis [19]	77.7	63.1	80.3	-	-	2103	62.1	68.8
BoT-SORT [10]	80.2	65.0	80.5	22521	86037	1212	65.5	71.2
Ours	81.1	65.4	80.6	22311	85971	1038	66.3	71.8

TABLE V

EVALUATION RESULTS AND COMPARISONS WITH THE STATE-OF-THE-ART-TRACKERS ON MOT20 TEST SET UNDER PRIVATE DETECTION PROTOCOLS.

Tracker	IDF1 \uparrow	HOTA \uparrow	MOTA \uparrow	FP \downarrow	FN \downarrow	IDSw \downarrow	AssA \uparrow	AssR \uparrow
SiamMOT [54]	69.1	-	67.1	-	-	-	-	-
FairMOT [8]	67.3	54.6	61.8	103440	88901	5243	54.9	60.7
TransCenter [36]	50.4	-	61.9	45895	146347	4653	37.0	45.1
TransTrack [13]	59.4	48.5	65.0	27197	150197	3608	45.2	51.9
CSTrack [52]	68.6	54.0	66.6	25404	144358	3196	54.0	57.6
RelationTrack [53]	70.5	56.5	67.2	61134	104597	4243	56.4	60.3
SOTMOT [55]	71.4	-	68.6	57064	101154	4209	-	-
MOTFR [32]	71.7	57.2	69.0	54894	101823	3648	57.1	62.6
FDTrack [33]	75.7	59.9	75.0	24011	102896	2226	-	-
OCSORT [22]	76.3	62.4	75.7	19067	105894	942	62.5	67.4
StrongSORT++ [34]	77.0	62.6	73.8	16632	117920	770	64.0	69.6
ByteTrack [9]	75.2	61.3	77.8	26249	87594	1223	59.6	66.2
Quo Vadis [19]	75.7	61.5	77.8	-	-	1185	59.9	67.0
BoT-SORT [10]	77.5	63.3	77.8	24638	88863	1257	62.9	68.6
Ours	78.6	64.1	77.9	25079	87943	1124	65.6	70.3

E. Benchmark Evaluation

We compare our OccluTrack with the state-of-the-art trackers on MOT17 and MOT20 datasets under private detection protocols, as shown in Table IV and Table V. Our OccluTrack consistently outperforms other state-of-the-art trackers across multiple important metrics.

a) MOT17: On the MOT17 dataset, our OccluTrack excels all other trackers in terms of five metrics, including IDF1, HOTA, MOTA, AssA, and AssR. Compared to our baseline tracker, BoT-SORT, our method consistently outperforms it on all metrics and achieves state-of-the-art performance. Regarding IDF1 and MOTA, our method improves 0.9% and 0.1% compared with our baseline, which indicates that our method has a more powerful tracking performance while keeping compatible detection performance. Correspondingly, the HOTA improved by 0.5%, considering both detection and tracking performance. Noticeably, the IDSw decreases by 14.2% from 1212 and reaches the optimal performance at 1038. Our method also surpasses all the other methods on AssA and AssR, showing more promising association ability. Although our method cannot achieve state-of-the-art performance on metrics like FP and FN compared with OC-

SORT [22] and ByteTrack [9], it still outperforms our baseline.

b) MOT20: Even though MOT20 is a more complex dataset with more crowdedness compared with the MOT17 dataset, our OccluTrack still achieves promising performance. Especially our proposed OccluTrack achieves better performance regarding IDF1, HOTA, MOTA, AssA, and AssR. For IDF1 and MOTA, OccluTrack improves them by 1.1% and 0.1%, corresponding to tracking performance and detection performance, contributing to 0.8% improvements on HOTA. This demonstrates that OccluTrack is superior in tracking while keeping good detection performance. In terms of association performance, our OccluTrack shows the best performance and achieves dramatic improvements, as high as 2.7% and 1.7% on AssA and AssR. While OccluTrack is not as good as OCSORT [22] and ByteTrack [9] on FP, FN, and IDSw, it still performs better than the baseline. Particularly for IDSw, our OccluTrack outperforms our baseline and reduces it by 10.6% from 1257 to 1124, showing more stable tracking performance.

F. Visualization

We conducted a comprehensive analysis of tracking results obtained from six videos in the MOT17 validation and test

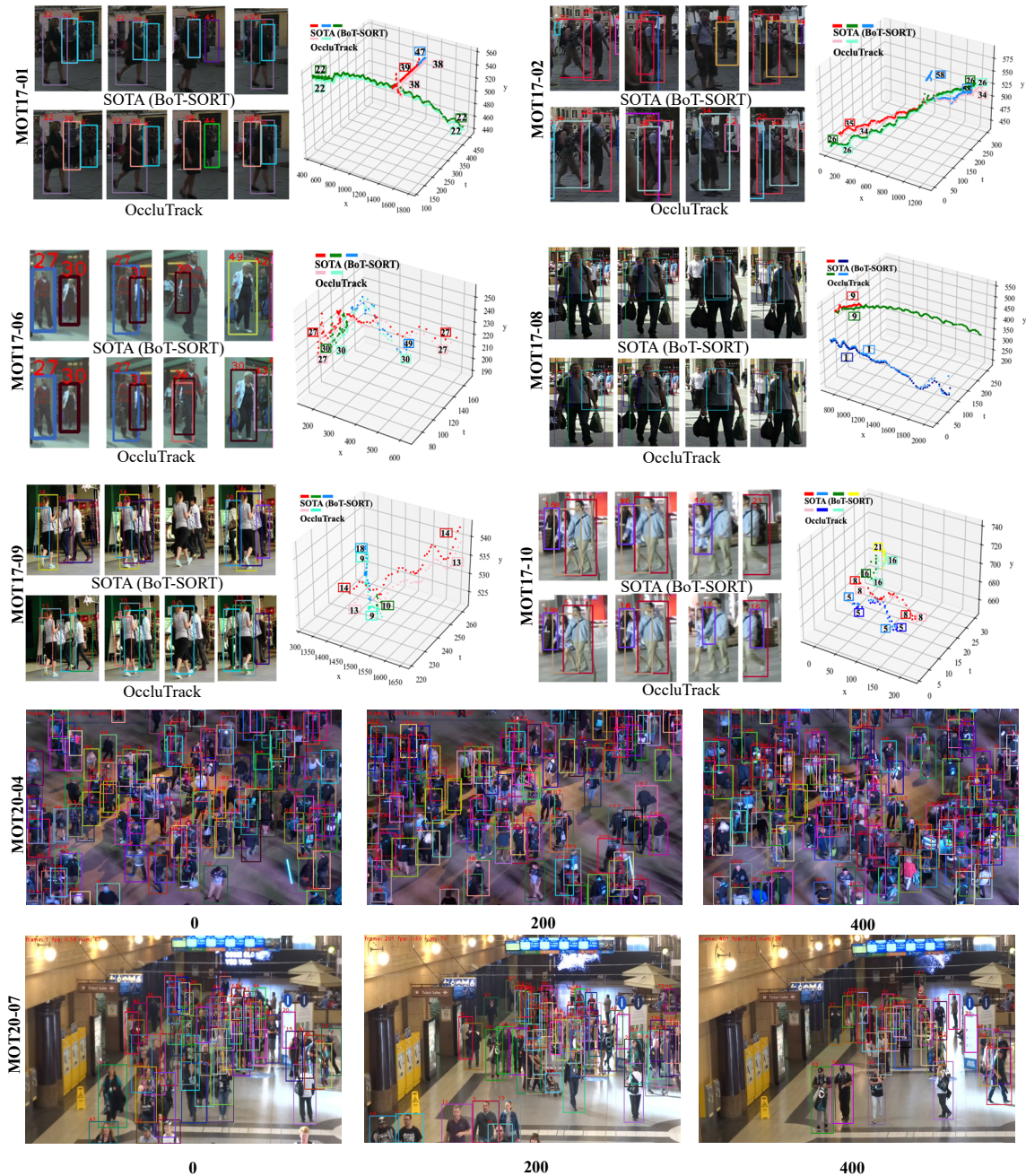


Fig. 6. Comparisons of BoT-SORT and our proposed OccluTrack on six samples from MOT17 and MOT20 datasets. On MOT17, we visualize sampled persons and corresponding trajectories to show the tracking performance. On MOT20, we show the sampled frames with selected video since it is hard to show the trajectories because of the crowdedness.

sets, as shown in Fig.6. Our purpose is to compare the tracking performance of our OccluTrack with that of the current state-of-the-art BoT-SORT under various conditions. We show the results of the two trackers when the selected pedestrians are before partial occlusion, during partial occlusion, during occlusion, and after occlusion. Besides, we demonstrate the trajectories for both trackers on the right of the figure.

As shown in Fig.6, BoT-SORT struggled to assign the correct ID to the person with ID 39, whose ID changed to 47 after occlusion. In contrast, our OccluTrack consistently tracked the same person with ID 38 throughout the sequence. This

discrepancy in performance can be attributed to the superior accuracy of OccluTrack’s predictions during occlusion, as they are closely aligned with the positions of occluded pedestrians. The visualized trajectories further confirm the robust tracking capability of our OccluTrack in maintaining track continuity for the person with ID 38. Similar trends were observed from other sub-figures, where our OccluTrack successfully tracked the person with ID 34 in MOT17-02-FRCNN, ID 30 in MOT17-06-FRCNN, ID 9 in both MOT17-08-FRCNN and MOT17-09-FRCNN, and ID 16 in MOT17-10-FRCNN, but BoT-SORT encountered difficulties.

In the MOT20 dataset, due to crowded scenes that limit visualization, we selected samples from all two videos in the test set to showcase the tracking performance of our OccluTrack. We sample three frames from each video at intervals of 200 frames and present the final tracking results in Fig.6. Due to the challenges posed by crowded scenes, it was not feasible to visualize individual trajectories or specific tracks. However, the visualization, combined with the corresponding numerical results in Section IV-E, shows the impressive tracking performance of our OccluTrack in handling crowded pedestrian tracking within the MOT20 dataset.

Our comprehensive evaluation of tracking results over MOT17 and MOT20 datasets demonstrates the superior tracking performance of our OccluTrack compared to SOTA. The visualizations provide evidence of OccluTrack's effectiveness in tackling occlusion challenges and accurately tracking pedestrians in different scenarios.

V. CONCLUSION

In conclusion, we have demonstrated that abnormal motion caused by partial occlusion is the missing key to enhancing multiple pedestrian tracking performance in IDF1 and IDSw. Our proposed OccluTrack can alleviate occlusion problems in multiple pedestrian tracking. By introducing an abnormal motion suppression mechanism, a pose-guided re-ID module, and an occlusion-aware distance measurement, we effectively mitigated the negative impact of partial occlusion on motion estimation, appearance features, and associations. Extensive evaluations showed OccluTrack outperforms state-of-the-art methods, particularly in IDF1, IDSw, HOTA, AssA, and AssR metrics.

REFERENCES

- [1] X. Wang, "Intelligent multi-camera video surveillance: A review," *Pattern recognition letters*, vol. 34, no. 1, pp. 3–19, 2013.
- [2] K. Wu, Y. Yang, Q. Liu, and X.-P. Zhang, "Focal stack image compression based on basis-quadtrees representation," *IEEE Transactions on Multimedia*, vol. 25, pp. 3975–3988, 2023.
- [3] I. Ahmed, S. Din, G. Jeon, F. Piccialli, and G. Fortino, "Towards collaborative robotics in top view surveillance: A framework for multiple object tracking by detection using deep learning," *IEEE/CAA Journal of Automatica Sinica*, vol. 8, no. 7, pp. 1253–1270, 2021.
- [4] B. Bescos, C. Campos, J. D. Tardós, and J. Neira, "Tightly-coupled multi-object tracking and slam," *IEEE robotics and automation letters*, vol. 6, no. 3, pp. 5191–5198, 2021.
- [5] D. Feng, C. Haase-Schütz, L. Rosenbaum, H. Hertlein, C. Glaeser, F. Timm, W. Wiesbeck, and K. Dietmayer, "Deep multi-modal object detection and semantic segmentation for autonomous driving: Datasets, methods, and challenges," *IEEE Transactions on Intelligent Transportation Systems*, vol. 22, no. 3, pp. 1341–1360, 2020.
- [6] X. Weng, J. Wang, D. Held, and K. Kitani, "3d multi-object tracking: A baseline and new evaluation metrics," in *2020 IEEE/RSJ International Conference on Intelligent Robots and Systems (IROS)*. IEEE, 2020, pp. 10 359–10 366.
- [7] A. Bewley, Z. Ge, L. Ott, F. Ramos, and B. Upcroft, "Simple online and realtime tracking," in *2016 IEEE international conference on image processing (ICIP)*. IEEE, 2016, pp. 3464–3468.
- [8] Y. Zhang, C. Wang, X. Wang, W. Zeng, and W. Liu, "Fairmot: On the fairness of detection and re-identification in multiple object tracking," *International Journal of Computer Vision*, vol. 129, pp. 3069–3087, 2021.
- [9] Y. Zhang, P. Sun, Y. Jiang, D. Yu, F. Weng, Z. Yuan, P. Luo, W. Liu, and X. Wang, "Bytetrack: Multi-object tracking by associating every detection box," in *Computer Vision–ECCV 2022: 17th European Conference, Tel Aviv, Israel, October 23–27, 2022, Proceedings, Part XXII*. Springer, 2022, pp. 1–21.
- [10] N. Aharon, R. Orfaig, and B.-Z. Bobrovsky, "Bot-sort: Robust associations multi-pedestrian tracking," *arXiv preprint arXiv:2206.14651*, 2022.
- [11] T. Meinhardt, A. Kirillov, L. Leal-Taixe, and C. Feichtenhofer, "Trackerformer: Multi-object tracking with transformers," in *Proceedings of the IEEE/CVF conference on computer vision and pattern recognition*, 2022, pp. 8844–8854.
- [12] F. Zeng, B. Dong, Y. Zhang, T. Wang, X. Zhang, and Y. Wei, "Motr: End-to-end multiple-object tracking with transformer," in *Computer Vision–ECCV 2022: 17th European Conference, Tel Aviv, Israel, October 23–27, 2022, Proceedings, Part XXVII*. Springer, 2022, pp. 659–675.
- [13] P. Sun, J. Cao, Y. Jiang, R. Zhang, E. Xie, Z. Yuan, C. Wang, and P. Luo, "Transtrack: Multiple object tracking with transformer," *arXiv preprint arXiv:2012.15460*, 2020.
- [14] P. Chu, J. Wang, Q. You, H. Ling, and Z. Liu, "Transmot: Spatial-temporal graph transformer for multiple object tracking," in *Proceedings of the IEEE/CVF Winter Conference on Applications of Computer Vision*, 2023, pp. 4870–4880.
- [15] Y. Zhang, H. Sheng, Y. Wu, S. Wang, W. Lyu, W. Ke, and Z. Xiong, "Long-term tracking with deep tracklet association," *IEEE Transactions on Image Processing*, vol. 29, pp. 6694–6706, 2020.
- [16] Z. Qin, S. Zhou, L. Wang, J. Duan, G. Hua, and W. Tang, "Motiontrack: Learning robust short-term and long-term motions for multi-object tracking," *arXiv preprint arXiv:2303.10404*, 2023.
- [17] X. Zhou, T. Yin, V. Koltun, and P. Krähenbühl, "Global tracking transformers," in *Proceedings of the IEEE/CVF Conference on Computer Vision and Pattern Recognition*, 2022, pp. 8771–8780.
- [18] L. Ke, X. Li, M. Danelljan, Y.-W. Tai, C.-K. Tang, and F. Yu, "Prototypical cross-attention networks for multiple object tracking and segmentation," *Advances in Neural Information Processing Systems*, vol. 34, pp. 1192–1203, 2021.
- [19] P. Dendorfer, V. Yugay, A. Osep, and L. Leal-Taixé, "Quo vadis: Is trajectory forecasting the key towards long-term multi-object tracking?" *Advances in Neural Information Processing Systems*, vol. 35, pp. 15 657–15 671, 2022.
- [20] Z. Wang, L. Zheng, Y. Liu, Y. Li, and S. Wang, "Towards real-time multi-object tracking," in *Computer Vision–ECCV 2020: 16th European Conference, Glasgow, UK, August 23–28, 2020, Proceedings, Part XI 16*. Springer, 2020, pp. 107–122.
- [21] E. Bochinski, V. Eiselein, and T. Sikora, "High-speed tracking-by-detection without using image information," in *2017 14th IEEE International Conference on Advanced Video and Signal Based Surveillance (AVSS)*, 2017, pp. 1–6.
- [22] J. Cao, X. Weng, R. Khirodkar, J. Pang, and K. Kitani, "Observation-centric sort: Rethinking sort for robust multi-object tracking," *arXiv preprint arXiv:2203.14360*, 2022.
- [23] X. Zhou, V. Koltun, and P. Krähenbühl, "Tracking objects as points," in *Computer Vision–ECCV 2020: 16th European Conference, Glasgow, UK, August 23–28, 2020, Proceedings, Part IV*. Springer, 2020, pp. 474–490.
- [24] X. Zhou, D. Wang, and P. Krähenbühl, "Objects as points," *arXiv preprint arXiv:1904.07850*, 2019.
- [25] J. Peng, C. Wang, F. Wan, Y. Wu, Y. Wang, Y. Tai, C. Wang, J. Li, F. Huang, and Y. Fu, "Chained-tracker: Chaining paired attentive regression results for end-to-end joint multiple-object detection and tracking," in *Computer Vision–ECCV 2020: 16th European Conference, Glasgow, UK, August 23–28, 2020, Proceedings, Part IV 16*. Springer, 2020, pp. 145–161.
- [26] J. Wu, J. Cao, L. Song, Y. Wang, M. Yang, and J. Yuan, "Track to detect and segment: An online multi-object tracker," in *Proceedings of the IEEE/CVF conference on computer vision and pattern recognition*, 2021, pp. 12 352–12 361.
- [27] J. Pang, L. Qiu, X. Li, H. Chen, Q. Li, T. Darrell, and F. Yu, "Quasi-dense similarity learning for multiple object tracking," in *Proceedings of the IEEE/CVF conference on computer vision and pattern recognition*, 2021, pp. 164–173.
- [28] N. Yang, Y. Wang, and L.-P. Chau, "Multi-object tracking with tracked object bounding box association," in *2021 IEEE International Conference on Multimedia & Expo Workshops (ICMEW)*. IEEE, 2021, pp. 1–6.
- [29] S. You, H. Yao, and C. Xu, "Multi-object tracking with spatial-temporal topology-based detector," *IEEE Transactions on Circuits and Systems for Video Technology*, vol. 32, no. 5, pp. 3023–3035, 2021.
- [30] Y. Zhou, Y. Wang, and L.-P. Chau, "Moving towards centers: Re-ranking with attention and memory for re-identification," *IEEE Transactions on Multimedia*, 2022.

- [31] N. Wojke, A. Bewley, and D. Paulus, "Simple online and realtime tracking with a deep association metric," in *2017 IEEE international conference on image processing (ICIP)*. IEEE, 2017, pp. 3645–3649.
- [32] J. Kong, E. Mo, M. Jiang, and T. Liu, "Motfr: Multiple object tracking based on feature recoding," *IEEE Transactions on Circuits and Systems for Video Technology*, vol. 32, no. 11, pp. 7746–7757, 2022.
- [33] Y. Jin, F. Gao, J. Yu, J. Wang, and F. Shuang, "Multi-object tracking: Decoupling features to solve the contradictory dilemma of feature requirements," *IEEE Transactions on Circuits and Systems for Video Technology*, 2023.
- [34] Y. Du, Z. Zhao, Y. Song, Y. Zhao, F. Su, T. Gong, and H. Meng, "Strongsort: Make deepsort great again," *IEEE Transactions on Multimedia*, 2023.
- [35] M. Chaabane, P. Zhang, J. R. Beveridge, and S. O'Hara, "Deft: Detection embeddings for tracking," *arXiv preprint arXiv:2102.02267*, 2021.
- [36] Y. Xu, Y. Ban, G. Delorme, C. Gan, D. Rus, and X. Alameda-Pineda, "Transcenter: Transformers with dense queries for multiple-object tracking," *arXiv e-prints*, pp. arXiv-2103, 2021.
- [37] Y. Zhang, T. Wang, and X. Zhang, "Motrv2: Bootstrapping end-to-end multi-object tracking by pretrained object detectors," *arXiv preprint arXiv:2211.09791*, 2022.
- [38] J. Gao, K.-H. Yap, Y. Wang, K. Garg, and B. S. Han, "Metformer: A motion enhanced transformer for multiple object tracking," in *2023 IEEE International Symposium on Circuits and Systems (ISCAS)*. IEEE, 2023, pp. 1–5.
- [39] N. Carion, F. Massa, G. Synnaeve, N. Usunier, A. Kirillov, and S. Zagoruyko, "End-to-end object detection with transformers," in *Computer Vision—ECCV 2020: 16th European Conference, Glasgow, UK, August 23–28, 2020, Proceedings, Part I 16*. Springer, 2020, pp. 213–229.
- [40] X. Zhu, W. Su, L. Lu, B. Li, X. Wang, and J. Dai, "Deformable detr: Deformable transformers for end-to-end object detection," *arXiv preprint arXiv:2010.04159*, 2020.
- [41] Z. Zhao, Z. Wu, Y. Zhuang, B. Li, and J. Jia, "Tracking objects as pixel-wise distributions," in *Computer Vision—ECCV 2022: 17th European Conference, Tel Aviv, Israel, October 23–27, 2022, Proceedings, Part XXII*. Springer, 2022, pp. 76–94.
- [42] Z. Ge, S. Liu, F. Wang, Z. Li, and J. Sun, "Yolox: Exceeding yolo series in 2021," *arXiv preprint arXiv:2107.08430*, 2021.
- [43] L. Tang, Y. Wang, and L.-P. Chau, "Weakly-supervised part-attention and mentored networks for vehicle re-identification," *IEEE Transactions on Circuits and Systems for Video Technology*, vol. 32, no. 12, pp. 8887–8898, 2022.
- [44] K. He, G. Gkioxari, P. Dollár, and R. Girshick, "Mask r-cnn," in *Proceedings of the IEEE international conference on computer vision*, 2017, pp. 2961–2969.
- [45] H. Zhang, C. Wu, Z. Zhang, Y. Zhu, H. Lin, Z. Zhang, Y. Sun, T. He, J. Mueller, R. Manmatha *et al.*, "Resnest: Split-attention networks," in *Proceedings of the IEEE/CVF Conference on Computer Vision and Pattern Recognition*, 2022, pp. 2736–2746.
- [46] H.-S. Fang, S. Xie, Y.-W. Tai, and C. Lu, "RMPE: Regional multi-person pose estimation," in *ICCV*, 2017.
- [47] K. Bernardin and R. Stiefelhagen, "Evaluating multiple object tracking performance: the clear mot metrics," *EURASIP Journal on Image and Video Processing*, vol. 2008, pp. 1–10, 2008.
- [48] P. Dendorfer, A. Osep, A. Milan, K. Schindler, D. Cremers, I. Reid, S. Roth, and L. Leal-Taixé, "Motchallenge: A benchmark for single-camera multiple target tracking," *International Journal of Computer Vision*, vol. 129, pp. 845–881, 2021.
- [49] M. Cordts, M. Omran, S. Ramos, T. Scharwächter, M. Enzweiler, R. Benenson, U. Franke, S. Roth, and B. Schiele, "The cityscapes dataset," in *CVPR Workshop on the Future of Datasets in Vision*, vol. 2, sn, 2015.
- [50] A. Ess, B. Leibe, K. Schindler, , and L. van Gool, "A mobile vision system for robust multi-person tracking," in *IEEE Conference on Computer Vision and Pattern Recognition (CVPR'08)*. IEEE Press, June 2008.
- [51] S. Shao, Z. Zhao, B. Li, T. Xiao, G. Yu, X. Zhang, and J. Sun, "Crowdhuman: A benchmark for detecting human in a crowd," *arXiv preprint arXiv:1805.00123*, 2018.
- [52] C. Liang, Z. Zhang, X. Zhou, B. Li, S. Zhu, and W. Hu, "Rethinking the competition between detection and reid in multiobject tracking," *IEEE Transactions on Image Processing*, vol. 31, pp. 3182–3196, 2022.
- [53] E. Yu, Z. Li, S. Han, and H. Wang, "Relationtrack: Relation-aware multiple object tracking with decoupled representation," *IEEE Transactions on Multimedia*, 2022.
- [54] B. Shuai, A. Berneshawi, X. Li, D. Modolo, and J. Tighe, "Siammot: Siamese multi-object tracking," in *Proceedings of the IEEE/CVF conference on computer vision and pattern recognition*, 2021, pp. 12 372–12 382.
- [55] L. Zheng, M. Tang, Y. Chen, G. Zhu, J. Wang, and H. Lu, "Improving multiple object tracking with single object tracking," in *Proceedings of the IEEE/CVF Conference on Computer Vision and Pattern Recognition*, 2021, pp. 2453–2462.